HHS Public Access

Author manuscript

MRS Bull. Author manuscript; available in PMC 2016 June 27.

Published in final edited form as:

MRS Bull. 2015 June ; 40(6): 480–489. doi:10.1557/mrs.2015.98.

Microscopy techniques for investigating the control of organic constituents on biomineralization

Coit T. Hendley IV, **Jinhui Tao**, **Jennie A.M.R. Kunitake**, **James J. De Yoreo**, and **Lara A. Estroff**

Abstract

This article addresses recent advances in the application of microscopy techniques to characterize crystallization processes as they relate to biomineralization and bio-inspired materials synthesis. In particular, we focus on studies aimed at revealing the role organic macromolecules and functionalized surfaces play in modulating the mechanisms of nucleation and growth. In nucleation studies, we explore the use of methods such as *in situ* transmission electron microscopy, atomic force microscopy, and cryogenic electron microscopy to delineate formation pathways, phase stabilization, and the competing effects of free energy and kinetic barriers. In growth studies, emphasis is placed on understanding the interactions of macromolecular constituents with growing crystals and characterization of the internal structures of the resulting composite crystals using techniques such as electron tomography, atom probe tomography, and vibrational spectromicroscopy. Examples are drawn from both biological and bio-inspired synthetic systems.

Keywords

Biomimetic (assembly); crystal; nucleation and growth; scanning probe microscopy; transmission electron microscopy

Introduction

One of the universal characteristics of biomineralizing systems is that macromolecular constituents, such as proteins and polysaccharides, are found in close association with the mineral constituents.[1,2] Some of these organic components are water soluble, but others assemble to create an insoluble scaffold within which the minerals form. This intimate relationship between the matrix and mineral, along with the unusual morphologies of biominerals and the common occurrence of metastable mineral phases, suggests that the organic matrix actively controls mineral nucleation and growth. Moreover, significant quantities of the organic matrix are typically occluded within the resulting hierarchically-structured tissues (discussed further in this issue by Schenk and Kim).[3] This composite architecture endows biominerals with remarkable mechanical properties and, as a result, during the past few decades, biomineral systems have inspired developments in materials synthesis of new composite materials.[4,5] However, truly emulating biological processes for

For table: [97–110]

novel material creation has yet to be fully realized, because both the mechanisms by which the macromolecular matrix assembles and mineralizes and the principles underlying the structure-function relationships of mineralized tissues are poorly understood. Recent advances in the application of microscopy techniques to define both the processes of matrix assembly and mineralization and the hierarchical distribution of matrix and mineral are beginning to fill the gaps in our understanding of both formation and properties. Here we review some of these advances, using examples from biological as well as bio-inspired systems to illustrate the insights they have enabled. Table I provides a summary of the microscopy techniques discussed, including their benefits and limitations within the scope of analyzing biominerals and bio-inspired systems.

Visualizing matrix assembly and mineral formation

What mechanisms and energetic factors control nucleation and growth?

In recent years, investigations of both matrix assembly and mineralization have been performed to better understand the *in vivo* mechanisms that control these processes. *In situ* methods have been particularly important, because dynamic behavior occurs in response to differences in energy states and the barriers that separate those states; thus, such studies provide an opportunity to probe the energy landscape across which matrix assembly and mineralization take place. For both processes, the important length scales are from the molecular scale to tens of nanometers. Consequently, atomic force microscopy (AFM) and transmission electron microscopy (TEM) have been the most significant techniques used, though the information gained is typically augmented with other types of data, both *in situ* and *ex situ*.

In situ AFM: Real-time imaging of assembly processes on surfaces

AFM is a type of scanning probe microscopy that uses a sharp tip on the end of a cantilever to sense changes in sample topography. When the tip is brought to within the range of the interatomic potential between the tip and surface, variations in the potential with position lead to vertical deflections of the cantilever. Thus the topography of the surface can be mapped by measuring the deflection of cantilever as the tip is raster-scanned over surface. Typically, this deflection is measured by reflecting a laser from the top of the cantilever onto a photodiode array, giving a vertical resolution of less than an Angstrom.

AFM can be applied to both organic matrices and mineral surfaces exposed to fluid, which is either static or flowing.[6,7] Consequently, it enables direct observations of matrix assembly on substrates,[8–10] mineral nucleation on organic matrices,[11,12] and post-nucleation growth and interaction with organic constituents.[7,13–15] These measurements can be complemented by a number of other techniques to obtain a comprehensive picture of chemical interactions, energetic drivers, and mechanisms of formation. The first, cryogenic electron microscopy (cryoEM), is a form of transmission electron microscopy (TEM) in which a sample of solution is frozen so rapidly in liquid N_2 or liquid ethane that it forms a thin layer of vitrified water. Cryo-EM enables the observation of specimens in their native environment without any staining or fixation, thus providing high-resolution structural information. The second, *in situ* dynamic force spectroscopy (DFS) is a special application of AFM that records the

force required to break the bond between a functionalized AFM tip and a surface. When this rupture force is measured as a function of the bond extension rate, the resulting relationship provides characteristic parameters of the intermolecular and mineral-matrix bonds such as the binding free energy per molecule. Vibrational and electronic spectroscopy can be used to the reveal the functional groups responsible for the observed changes in free energies and barriers, and molecular simulations can be employed to test proposed mechanisms and determine underlying structural reasons for the dominant interactions.

AFM has been used to investigate assembly of protein matrices by introducing aqueous solutions of protein into a sample chamber referred as a fluid cell, which contains substrates that promote assembly.[8,9] *In vivo,* collagen molecules, which form the organic matrix of bone, align and intertwine to form microfibrils containing "hole zones," where there are gaps between the N- and C-termini of successive collagen molecules.[16] Observations of collagen assembly on mica revealed formation of ordered fibrils via two distinct steps that resulted in the same periodicity observed in collagen fibrils formed *in vivo* (Figure 1A–F).[8] First, three single strand collagen molecules associate with one another to form 1.5 nm-high triple-helices called topocollagen molecules. These then assembled into ordered, 3 nm-high microfibrils, which formed the building blocks of the larger scale fibrils. Other studies recorded development of alternative architectures that depended strongly on the choice of pH and salt concentration (Figure 1G–I). For example, while the ordered structure seen in Figure 1A-F is obtained at pH 9.0 for K^+ concentrations of 200 mm and above, at pH 4.0 the architecture evolves from a monolayer of randomly oriented molecules to a monolayer of co-aligned molecules to 3D bundles of co-aligned molecules as the K^+ concentration is increased from 100 to 300 mM.[10] Comparing the *in situ* results with coarse-grained molecular models of assembly provided insights into the energetic underpinnings of collagen architecture.[10] Predictions based on variations of the relative strengths of the inter-collagen and collagen-substrate binding through a periodic set of strong and weak inter-collagen binding sites gave the observed evolution in collagen architecture.

Mineral nucleation on organic matrices can also be visualized by AFM.[11,12] Organic matrices are first assembled on flat substrates. Aqueous solutions of the mineral phase are then passed through the fluid cell and formation of mineral nuclei is observed (Figure 1J–L). If the nucleation process is arrested by switching from flow of reagents to a liquid in which the mineral has no solubility, such as alcohol, the sample can be collected and analyzed by TEM or Raman spectroscopy to determine the mineral phase at a single point in time.[11] The use of DFS to measure the binding energy of the protein to single crystal substrates of the mineral allows one to correlate the interfacial energy with matrix-mineral binding free energy.[12,17,18]

In bone, nonstoichiometric hydroxyapatite ($Ca_{10}(PO_4)_6(OH)_2$; HA) crystals form within a highly organized matrix of collagen.[19] There is an ongoing debate regarding the nucleating potential of collagen fibrils in the absence of any other proteins.[20–22] Recently, AFM measurements of heterogeneous calcium phosphate nucleation rates on collagen showed that solutions stable for days in the absence of collagen produced nuclei in hours or less on collagen matrices.[11] At supersaturations below the solubility limit of amorphous calcium phosphate (ACP), HA formed directly, but when the concentration was raised to slightly

above the solubility limit of ACP, the amorphous phase formed first (Figure 1J) before transforming to octacalcium phosphate ($Ca_8H_2(PO_4)_6 \cdot 5H_2O$; OCP) (Figure 1K) and, finally, HA (Figure 1L). Analysis of nucleation rates (Figure 1M) gave interfacial energies two to three times less than those estimated for homogeneous nucleation and barriers that were smaller by more than an order of magnitude. Analysis of the size distribution of particles that, on average, grew versus those that dissolved (Figure 1N), provided an estimate of the critical nucleus size. However, neither the change from HA nucleation to ACP nucleation nor the small values of critical size could be understood within classical nucleation theory. Comparison to cryoEM and titration analyses revealed a formation pathway involving assembly of multi-ion complexes, which offered a rationale for the unexpected formation of ACP precursor particles and the low value of the critical size.

Cryogenic Electron Microscopy (cryoEM) and tomography: High-resolution, three-dimensional (3D) imaging of hydrated samples

CryoEM techniques[23] can provide insights into tissue structures at close to native state.[24] They can also be used to provide quasi-time resolved studies of nucleation and growth processes.[25–27] These studies can complement *in situ* AFM studies, and provide a more detailed picture of mineralization occurring *within* an organic matrix. For example, cryoEM studies of synthetic intrafibrillar HA formation in collagen fibrils revealed the early stages of infiltration of ACP particles at the hole zones in the fibrils (Figure 2A,B).[28] CryoEM tomography of the fully mineralized fibrils revealed embedded nm-thick plate-shaped HA crystals with their *c*-axis parallel to the fibril axis. Similar cryoEM approaches have been taken to study other composite systems such as calcium carbonate nucleation under Langmuir–Blodgett monolayers.[25,29] In these studies, amorphous calcium carbonate (ACC) forms and then transforms to either calcite (in the absence of the monolayer) or vaterite and then calcite (with the monolayer present) by dissolution/reprecipitation.[25]

In situ TEM: Direct observation of nucleation in bulk solutions and within organic matrices

When nucleation occurs in bulk solution or within a biomimetic matrix, AFM cannot be used to observe the nucleation process. *In situ* liquid phase TEM provides a novel technique in these instances.[30–33] A sealed liquid cell on a specialized TEM holder (Figure 3A,B) allows for mixing reagents at the entrance to the cell and flow of the mixture through the cell.[34] Alternatively, the cell can be filled with one reagent through one of the two flow lines, and the second reagent can be introduced by gaseous diffusion through the second line.[35] To observe nucleation within a macromolecular matrix, the macromolecules are added to one of the two reagents and transferred into the cell prior to introduction of the second reagent. The appearance of mineral nuclei and the spatial relationship to an organic matrix can then be observed by TEM imaging. Electron diffraction is used to determine the phase of the mineral and its evolution. Low-dose methods, beam shuttering, and examination of regions not previously exposed to the beam are required to separate electron beam effects from intrinsic phenomena.[36,37] Liquid phase TEM was used to observe calcium carbonate ($CaCO_3$) nucleation both in organic-free solutions[34] and in the presence of an organic matrix.[35] Results on pure solutions produced by mixing of two aqueous reagents demonstrated that multiple nucleation pathways can be simultaneously operative, including

formation both directly from solution and indirectly through transformation of initially formed amorphous or crystalline precursors.[34] When crystalline phases formed as secondary phases through transformation of primary ACC, the secondary nuclei appeared at the surface of the ACC particles and remained in direct contact until the ACC was consumed. When ACC dissolution was induced, the observed behavior suggested ACC comprises a spectrum of structures ranging from dense liquids to solids.

To investigate the role of macromolecular matrices in directing mineralization, liquid phase TEM was also used to observe the nucleation and growth of $CaCO_3$ in the presence of poly(styrene sulfonate) (PSS).[35] This acidic macromolecule was chosen to mimic the polysaccharides believed important in the formation of certain marine biominerals.[38–40] In the PSS-free system, the configuration used for these experiments led to random nucleation with vaterite, a metastable $CaCO_3$ polymorph, being the dominant phase. When PSS was first introduced in the $CaCl_2$ reagent, calcium binding to the polymer resulted in formation of Ca-PSS globules with an average diameter of approximately 10 nm (Figure 3C). These observations were complemented by titration calorimetry, which showed that more than 50% of the Ca^{2+} ions were complexed by PSS, zeta potential measurements (Figure 3D), and *in situ* Fourier transform infrared spectroscopy (FTIR), which demonstrated that the Ca^{2+} ions bound to the sulfate groups. Upon introduction of carbonate, ACC particles nucleated first but only formed within the globules (Figure 3C–F). Vaterite appeared at much later times but only formed outside of the globules. Both phases grew at diffusion-limited rates (Figure 3E), from which the supersaturation at the time of nucleation could be determined. The findings demonstrated that ion binding can play a significant role in directing nucleation, independent of any control over interfacial free-energy, and that the acidic polymers redirect the nucleation pathway to ACC formation.

Macromolecular inclusions in biominerals and bioinspired materials

How are large additives incorporated into crystalline lattices?

Understanding the internal structure of biominerals, and the interactions between biomacromolecules and growing inorganic crystals, is of great interest for developing bio-inspired synthetic materials with improved property profiles, as discussed in more detail in the article by Schenck and Kim in this issue. One outstanding challenge is the compositional and structural characterization of hierarchically-structured, hydrated, biomineralized tissues, which typically have significant quantities of nonperiodically arranged organics occluded within crystalline matrices. While *in situ* techniques provide insights into the very early stages of crystal nucleation and growth, due to sample size limitations of AFM fluid cells and *in situ* TEM, the final product cannot be structurally characterized. Additionally, for biological tissues, we often only have the final mineral product since we currently cannot image the formation processes *in vivo*.

Fortunately, in recent years, advanced characterization techniques have provided unprecedented resolution of the internal structure of biominerals and unique insights into the mechanisms of formation of these structures. The most useful techniques enable simultaneous imaging of the organic and inorganic components, with nanometer-scale resolution, and when possible, chemically rich information.

Electron Tomography: 3D structural information

Electron microscopy, in particular scanning TEM (STEM), is particularly well-suited to simultaneously imaging organic and inorganic components with nanometer-scale resolution.[41] In addition, local crystallographic information can be obtained by selected-area electron diffraction (SAED), and where possible, high-resolution lattice imaging can provide additional insight into crystal structure.[42] Immunogold labeling can be used in conjuation with TEM to visualize the locations of specific proteins within a tissue sample.[43–46] Briefly, small (<10 nm) gold nanoparticles are functionalized with antibodies and allowed to bind to the target proteins within tissue thin sections. The high electron density of the gold nanoparticles facilitates imaging by TEM.

More recently, electron tomography, in which a series of images of the sample are taken at varying tilt angles with respect to the electron beam and reconstructed into a 3D image of the sample,[47,48] has emerged as a technique for obtaining additional spatial information about the distribution of organic inclusions within biominerals. Energy dispersive spectroscopy (EDS) and electron energy-loss spectroscopy (EELS) can provide additional chemical information about the samples, but both techniques require high accelerating voltages. One of the main challenges in performing these types of experiments on biomineralized tissues is that samples must be electron transparent, which often requires thinning of samples via focused ion beam (FIB) milling. As alternatives to FIB, other techniques can be used to obtain ultrathin sections such as cutting with a (cryo)ultramicrotome or wedge polishing hard tissue samples.[17,49] Additionally, beam damage can be a problem for samples with high organic content as it can introduce imaging artifacts such as amorphization of crystalline regions, crystallization of amorphous regions, and destruction of organic regions.

Mollusk shells are a model biomineral that have been extensively studied due to their dramatically higher hardness and fracture toughness as compared to geologic minerals.[50] Electron microscopy and tomography have revealed details regarding the incorporation of biomacromolecules within the $CaCO_3$ single crystals that make up both the prismatic (calcitic) and nacreous (aragonitic) layers.[51–53] In all of these studies, a common picture emerges of single-crystal components (from SAED) with nanoscale inclusions, which are often arranged along preferred crystallographic orientations (from electron tomography). In another study, a combination of annular dark field STEM, electron tomography, SAED, and EELS were used to analyze the remarkably structured calcite building blocks of coccolithophores (single-celled algae).[54]

Inspired by biominerals such as mollusk shells, there have been several recent studies on the incorporation of nanoscale aggregates of organic macromolecules into synthetic single crystals of calcite (see Schenck and Kim article for additional discussion).[55,56] The internal structure of calcite crystals grown within an agarose gel was revealed by electron tomography (Figure 2c–e). Similar to biogenic crystals, the presence of the nanoscale gel fibers within the crystal did not appear to disrupt the local crystalline structure. Even more interestingly, the cavities in which the fibers were encased appeared to be faceted and contained high-energy homocharged {012} facets as well as the expected {104} cleavage planes.

These studies reveal the power of electron tomography for revealing the internal structure of biominerals and bio-inspired crystals. What these static techniques cannot capture, however, are the mechanisms by which the organic macromolecules become trapped within the crystals without significantly disrupting the lattice. Future studies will aim to apply AFM, cryoEM and/or liquid cell TEM to visualize the growth of crystals in the presence of these nanoscale additives.

Atom Probe Tomography (APT): Spatially-resolved chemical information at the nanoscale

Atom probe tomography offers both 3D imaging and chemical composition measurements at the atomic scale (around 0.1-0.3 nm resolution in depth and 0.3-0.5 nm laterally).[57,58] This technique is currently the only way to chemically map inclusions in biominerals, in detail, at the nanoscale. Using FIB and nanomanipulators, needle-shaped samples are milled and mounted to a Si post array. Then a pulsed ultraviolet laser sequentially triggers field evaporation of single atoms or small clusters from the surface of the tip. The resulting ions are projected onto a position sensitive detector (PSD) and their time-of-flight, and thus chemical identity, is determined. The detector simultaneously measures 1) the time between the laser flash and the arrival on the PSD to determine the mass over charge ratio of the ions and 2) the X-Y position and the order of arrival of the ions on the PSD to reconstruct the original position of the atoms in the sample. By repeating this operation, the atoms are progressively removed from the sample, and a 3D image of the material can be reconstructed at the atomic scale (Figure 4A). The small size of the sample, however, limits the overall image size and since the ejected organic fragments tend to be larger than single ions, the resolution of their location is slightly reduced. Though this technique was originally developed for studies of metals and semiconductors, recent advancements have made studies of composite and biological materials possible[58–60] and, despite challenges, the results reported so far are groundbreaking.

The first pioneering application of APT to the study of biomineral composites was to the tooth of a chiton, a small marine mollusk whose teeth are designed to scrape algae off of rocks.[61] Their teeth have a hard magnetite exterior and several organic-inorganic interfaces that are of interest. The APT revealed a 2–4 nm boundary-like region where the organic and inorganic materials are interspersed. The authors speculate that this interphase likely improves adhesion between the chemically disparate regions. A similar approach has been applied to dentin from elephant teeth.[62] APT revealed long organic fibers running parallel to the tooth direction with cross-sectional dimensions on the order of the width of a collagen microfibril (Figure 4b). They also found that the fibers have locally increased concentrations of Mg^{2+} and Na^{+} ions (Figure 4c–d) and theorize that the exterior of the fibers may be coated with noncollagenous proteins, which selectively bind ions and may aid in mineralization. In other work, details of the chemical composition and spatial heterogeneity of rodent enamel have been elucidated using APT.[63] The unique chemical insights from APT allow for conclusions to be drawn about mechanisms of biomineral formation and function based on spatially resolved chemical information.

X-ray spectroscopy: Mapping amorphous to crystalline transformations

X-ray spectroscopy techniques, including x-ray absorption fine structure (EXAFS) and x-ray absorption near-edge spectroscopy (XANES), coupled with x-ray photoelectron emission microscopy (X-PEEM), have yielded many insights into the structures of biominerals.[64–68] Sample preparation is relatively minimal compared to other techniques (typically embedding in resin and polishing), but some of the techniques are surface-sensitive (depending on the wavelength of x-rays used), requiring additional attention to avoid artifacts from surface-layers left by polishing.

EXAFS spectra contain information about local structure and therefore can distinguish between amorphous and crystalline phases. X-PEEM studies have provided a detailed picture of the amorphous to crystalline transformation in a variety of biomineralized tissues. The use of amorphous precursors in biomineralization has attracted much attention as a synthetic route to morphologically complex single crystals.[69] For example, a recent study of larval sea urchin spicules, mineralized skeletal components, revealed that ACC nanoparticles unexpectedly persisted despite crystallization of the surrounding material.[70] To-date, most studies have focused on characterizing the inorganic component of biominerals, however, the organic component can also be probed by looking at the carbon K-edge in the EXAFS spectra, as shown in several recent studies.[71–73]

Vibrational spectromicroscopy: Chemically rich 3D maps of tissue composition

Vibrational (Raman and infrared) spectromicroscopy can non-destructively provide spatially-resolved (at the micrometer scale) compositional information about the organic and inorganic components of biominerals.[74,75] These techniques couple a Raman (or IR) spectrometer to a standard optical microscope, allowing imaging of a sample and Raman (or IR) analysis with a microscopic laser spot. Two-dimensional maps of tissue samples are typically generated by raster-scanning the laser over a selected area to generate a 2D area map with a spectrum at each pixel. Both organic matrix and inorganic mineral components have distinct spectral signatures. Confocal Raman microscopy refers to the ability to spatially filter the analysis volume of the sample, in the XY (lateral) and Z (depth) axes. The limits of spatial resolution are defined principally by the laser quality and wavelength and the type of microscope objective. Typical spatial resolution is on the order of 0.5-1 μm.

Stomatopod raptorial appendages, which are used by the organism to “club” or “spear” prey, (depending on the species) at very high velocities,[76] have recently been analyzed by Raman microscopy.[77] In this study, confocal Raman microscopy was used to map the compositional gradients present in these unique appendages, These maps revealed a transition from ACC to amorphous calcium phosphate at the bulk-impact interface, and finally, to highly crystalline sulfate-containing fluorapatite (FAP) along the actual impact surface. Importantly, the sensitivity of the Raman technique allowed discernment of FAP from apatite, which could not be done on the basis of standard x-ray diffraction alone.

Confocal Raman spectromicroscopy can also be used to characterize compositional changes within 3D structures.[78–81] In addition to 2D and 3D compositional maps, polarized Raman spectroscopy can provided quantification of molecular and crystallographic orientation. For

example, Masic et al. were able to observe multiscale orientational changes in rat tail tendon (Type I) collagen under stress using polarized Raman spectroscopy.[82] Finally, one of the most promising applications of Raman is *in vivo* imaging, and the capability to couple Raman microscopes with other techniques, such as fluorescence microscopy. For example, bone formation in zebrafish larvae was recently observed *in vivo*.[83,84] Anesthetized fish were analyzed under a water-immersion objective, using a fluorescence-enabled modified Raman setup. Spectra were acquired along growing bones in the fin rays and showed a clear transition from little or no calcium phosphate to a predominance of calcium phosphate, correlated with calcium fluorescence (a calcium-binding marker). Furthermore, the peaks suggested that octacalcium phosphate (OCP), or an OCP-like intermediate phase, may be present, a finding previously undocumented *in vivo*.

Conclusion

The development and application of advanced microscopy and spectroscopy techniques, some of which can be performed *in situ*, have been essential for understanding the structure and formation of biominerals and bio-inspired materials. The information provided by these techniques about the chemistry, crystallography, phase distribution, structure, energetics, and kinetics of these materials forms the basis for an increasingly diverse understanding of the fundamental mechanisms by which natural systems can create structures. Yet we are only beginning to effectively mimic these processes synthetically. Fully understanding incorporated organic materials and the role they play in composite crystals will lead to further developments at the leading edge of characterization and synthesis.

Numerous recent advances in AFM imaging promise to provide new insights into biomineralization processes. High speed imaging[85–87] with image collection times below 100 ms should enable researchers to probe the conformational fluctuations and transformations that control the emergence of order during the assembly of an organic matrix. Frequency Modulated AFM (FM-AFM)[88–90] is capable of both imaging the structure of the near-surface water layers at solid interfaces in solutions and measuring the small attractive forces barriers between the tip and sample during the approach to the surface. These capabilities will lead to new insights into the role of solvation forces and solvent-mediated matrix-mineral interactions in directing biomineral formation.

Several of the techniques described in this review, such as liquid phase TEM, are still in their infancy. Development of liquid cells for TEM instrumented for pH measurement, heating and cooling, and quantitative mixing will enable a wider range of experiments with well-defined solution saturation states. Solution supersaturation is a critical parameter to quantify in order for the resulting data regarding nucleation and growth modes to be interpreted in terms of theoretical predictions or compared to computer simulations.

New techniques, beyond those described here, are also emerging that have the potential to provide even more detailed spatial and temporal resolution of biomineralization processes in hydrated (fluid) environments. For example, the recent implementation of scanning transmission x-ray microscopy end stations on synchrotron sources with resolution down to 10–20 nm[91] has enabled elemental mapping of hybrid organic/inorganic structures in

fluid.[92,93] Another development is a new type of scanning electron microscope (e.g., airSEM™) in which fully-hydrated and uncoated samples can be imaged in air, allowing *in situ* observation of processes, such as calcium transport, in living organisms.[84,94] The airSEM enables correlative imaging of tissues under ambient conditions by light and fluorescence microscopy and electron microscopy with elemental analysis by EDS.[83,95] Finally, new sample preparation techniques such as cryo-FIB, in which cryogenically frozen samples are thinned by a focused ion beam will enhance our ability to prepare electron-transparent samples of biological samples under near-native conditions.[96]

The future holds the promise of integrating several of these techniques to allow for correlative imaging and, for example, link structural and compositional variations to changes in properties, such as elastic moduli or hardness. Ultimately, the knowledge gained through such studies will enable materials scientists to reproduce the remarkable properties of biominerals through bio-inspired approaches to materials synthesis.

Acknowledgments

The authors acknowledge support from the National Science Foundation (DMR 1210304) and the National Institutes of Health (CA173083). Additional support for this work was provided by the US Department of Energy, Office of Basic Energy Sciences, Materials Science and Engineering Division, as well as the Laboratory Directed Research and Development Initiative on Materials Synthesis and Simulation across Scales, at the Pacific Northwest National Laboratory (PNNL). PNNL is operated by Battelle for the US Department of Energy under Contract DE-AC05–76RL01830.

References

1. Lowenstam, H.; Weiner, S. On Biomineralization. Oxford University Press Inc; 1989.
2. Dove, PM.; De Yoreo, JJ.; Weiner, S., editors. Mineral Society of America. Washington, DC: 2003. p. 54
3. Asenath-Smith E, Li H, Keene EC, Seh ZW, Estroff La. Adv Funct Mater. 2012; 22(14):2891–2914.
4. Nudelman F, Sommerdijk NaJ. M Angew Chemie - Int Ed. 2012; 51:6582–6596.
5. Arakaki A, Shimizu K, Oda M, Sakamoto T, Nishimura T, Kato T. Org Biomol Chem. 2014; 13(4): 974–989. [PubMed: 25375353]
6. Franz CM, Muller DJ. Methods Mol Biol. 2011; 736:97–107. [PubMed: 21660723]
7. De Yoreo, JJ. AIP Conference Proceedings. Vol. 916. AIP; 2007. p. 416-438.
8. Cisneros DA, Hung C, Franz CM, Muller DJ. J Struct Biol. 2006; 154(3):232–245. [PubMed: 16600632]
9. Chung S, Shin SH, Bertozzi CR, De Yoreo JJ. Proc Natl Acad Sci U S A. 2010; 107(38):16536–16541. [PubMed: 20823255]
10. Narayanan B, Gilmer GH, Tao J, De Yoreo JJ, Ciobanu CV. Langmuir. 2014; 30(5):1343–1350. [PubMed: 24437511]
11. Habraken WJEM, Tao J, Brylka LJ, Friedrich H, Bertinetti L, Schenk AS, Verch A, Dmitrovic V, Bomans PHH, Frederik PM, Laven J, van der Schoot P, Aichmayer B, de With G, DeYoreo JJ, Sommerdijk NAJM. Nat Commun. 2013; 4:1507. [PubMed: 23422675]
12. Hamm LM, Giuffre AJ, Han N, Tao J, Wang D, De Yoreo JJ, Dove PM. Proc Natl Acad Sci U S A. 2014; 111(4):1304–1309. [PubMed: 24434555]
13. Rimer JD, An Z, Zhu Z, Lee MH, Goldfarb DS, Wesson JA, Ward MD. Science. 2010; 330(6002): 337–341. [PubMed: 20947757]
14. Orme, Ca; Noy, a; Wierzbicki, a; Mc Bride, MT.; Grantham, M.; Teng, HH.; Dove, PM.; De Yoreo, JJ. Nature. 2001; 411(6839):775–779. [PubMed: 11459051]
15. Olafson KN, Ketchum MA, Rimer JD, Vekilov PG. Proc Natl Acad Sci U S A. 2015:1501023112.

16. Orgel JPRO, Irving TC, Miller A, Wess TJ. Proc Natl Acad Sci U S A. 2006; 103(24):9001–9005. [PubMed: 16751282]
17. Tao J, Battle KC, Pan H, Salter EA, Chien YC, Wierzbicki A, De Yoreo JJ. Proc Natl Acad Sci U S A. 2014; 112(2):326–331. [PubMed: 25540415]
18. De Yoreo JJ, Chung S, Friddle RW. Adv Funct Mater. 2013; 23(20):2525–2538.
19. Weiner S, Wagner HD. Annu Rev Mater Sci. 1998; 28(1):271–298.
20. Landis WJ, Silver FH. Cells Tissues Organs. 2009; 189(1-4):20–24. [PubMed: 18703872]
21. Wang Y, Azaïs T, Robin M, Vallée A, Catania C, Legriel P, Pehau-Arnaudet G, Babonneau F, Giraud-Guille MM, Nassif N. Nat Mater. 2012; 11(8):724–733. [PubMed: 22751179]
22. Olszta MJ, Cheng X, Jee SS, Kumar R, Kim YY, Kaufman MJ, Douglas EP, Gower LB. Mater Sci Eng R Reports. 2007; 58(3-5):77–116.
23. Nudelman F, de With G, Sommerdijk NAJM. Soft Matter. 2011; 7(1):17.
24. Quan BD, Sone ED. Methods Enzymol. 2013; 532:189–205. [PubMed: 24188768]
25. Pichon BP, Bomans PHH, Frederik PM, Sommerdijk NAJM. J Am Chem Soc. 2008; 130(12): 4034–4040. [PubMed: 18303894]
26. Carcouët CCMC, van de Put MWP, Mezari B, Magusin PCMM, Laven J, Bomans PHH, Friedrich H, Esteves ACC, Sommerdijk NAJM, van Benthem RATM, de With G. Nano Lett. 2014; 14(3): 1433–1438. [PubMed: 24499132]
27. Frandsen C, Legg BA, Comolli LR, Zhang H, Gilbert B, Johnson E, Banfield JF. CrystEngComm. 2014; 16(8):1451–1458.
28. Nudelman F, Pieterse K, George A, Bomans PHH, Friedrich H, Brylka LJ, Hilbers PAJ, de With G, Sommerdijk NAJM. Nat Mater. 2010; 9(12):1004–1009. [PubMed: 20972429]
29. Pouget EM, Bomans PHH, Goos JACM, Frederik PM, de With G, Sommerdijk NAJM. Science. 2009; 323(5920):1455–1458. [PubMed: 19286549]
30. Williamson MJ, Tromp RM, Vereecken PM, Hull R, Ross FM. Nat Mater. 2003; 2(8):532–536. [PubMed: 12872162]
31. Wang CM, Liao HG, Ross FM. MRS Bull. 2015; 40(01):46–52.
32. Zheng H, Meng YS, Zhu Y. MRS Bull. 2015; 40(01):12–18.
33. Sutter EA, Sutter PW. J Am Chem Soc. 2014; 136(48):16865–16870. [PubMed: 25407028]
34. Nielsen MH, Aloni S, De Yoreo JJ. Science (80-). 2014; 345(6201):1158–1162.
35. Smeets PJM, Cho KR, Kempen RGE, Sommerdijk NAJM, De Yoreo JJ. Nat Mater. 2015 advance on.
36. Woehl TJ, Evans JE, Arslan I, Ristenpart WD, Browning ND. ACS Nano. 2012; 6(10):8599–8610. [PubMed: 22957797]
37. Zhang H, De Yoreo JJ, Banfield JF. ACS Nano. 2014; 8(7):6526–6530. [PubMed: 25000275]
38. Addadi L, Moradian J, Shay E, Maroudas NG, Weiner S. Proc Natl Acad Sci. 1987; 84(9):2732–2736. [PubMed: 16593827]
39. Marsh ME. Protoplasma. 1994; 177(3-4):108–122.
40. Schenk AS, Zlotnikov I, Pokroy B, Gierlinger N, Masic A, Zaslansky P, Fitch AN, Paris O, Metzger TH, Cölfen H, Fratzl P, Aichmayer B. Adv Funct Mater. 2012; 22(22):4668–4676.
41. Sousa, Aa; Leapman, RD. Ultramicroscopy. 2012; 123:38–49. [PubMed: 22749213]
42. Kabalah-Amitai L, Mayzel B, Kauffmann Y, Fitch AN, Bloch L, Gilbert PUPA, Pokroy B. Science. 2013; 340(6131):454–457. [PubMed: 23620047]
43. Osuna-Mascaró A, Cruz-Bustos T, Benhamada S, Guichard N, Marie B, Plasseraud L, Corneillat M, Alcaraz G, Checa A, Marin F. Comp Biochem Physiol B Biochem Mol Biol. 2014; 168:76–85. [PubMed: 24291423]
44. Mass T, Drake JL, Peters EC, Jiang W, Falkowski PG. Proc Natl Acad Sci U S A. 2014; 111(35): 12728–12733. [PubMed: 25139990]
45. Ameye L, Hermann R, Killian C, Wilt F, Dubois P. J Histochem Cytochem. 1999; 47(9):1189–1200. [PubMed: 10449540]
46. Seto J, Zhang Y, Hamilton P, Wilt F. J Struct Biol. 2004; 148:123–130. [PubMed: 15363792]
47. Midgley PA, Weyland M. Ultramicroscopy. 2003; 96(3-4):413–431. [PubMed: 12871805]

48. Leary R, Midgley P, Thomas J. Accounts Chem …. 2012; 45(10)
49. Voyles PM, Grazul JL, Muller DA. Ultramicroscopy. 2003; 96(3-4):251–273. [PubMed: 12871793]
50. Kunitake ME, Mangano LM, Peloquin JM, Baker SP, Estroff LA. Acta Biomater. 2013; 9(2):5353–5359. [PubMed: 23036948]
51. Li H, Xin HL, Kunitake ME, Keene EC, Muller Da, Estroff La. Adv Funct Mater. 2011; 21(11): 2028–2034.
52. Gries K, Kröger R, Kübel C, Fritz M, Rosenauer A. Acta Biomater. 2009; 5(8):3038–3044. [PubMed: 19427933]
53. Okumura T, Suzuki M, Nagasawa H, Kogure T. J Cryst Growth. 2013; 381:114–120.
54. van de Locht R, Slater TJAT, Verch A, Young JR, Haigh SJ, Kröger R. Cryst Growth Des. 2014:140320115609006.
55. Li H, Xin HL, Muller Da, Estroff La. Science. 2009; 326(5957):1244–1247. [PubMed: 19965470]
56. Kim YY, Ganesan K, Yang P, Kulak AN, Borukhin S, Pechook S, Ribeiro L, Kröger R, Eichhorn SJ, Armes SP, Pokroy B, Meldrum FC. Nat Mater. 2011; 10(11):890–896. [PubMed: 21892179]
57. Seidman DN. Annu Rev Mater Res. 2007; 37(1):127–158.
58. Miller MK, Forbes RG. Mater Charact. 2009; 60(6):461–469.
59. Kelly TF, Nishikawa O, Panitz Ja, Prosa TJ. MRS Bull. 2009 Oct.34:744–750.
60. Marquis EA, Bachhav M, Chen Y, Dong Y, Gordon LM, McFarland A. Curr Opin Solid State Mater Sci. 2013; 17(5):217–223.
61. Gordon LM, Joester D. Nature. 2011; 469(7329):194–197. [PubMed: 21228873]
62. Gordon L, Tran L, Joester D. ACS Nano. 2012; No. 12:10667–10675. [PubMed: 23176319]
63. Gordon LM, Cohen MJ, MacRenaris KW, Pasteris JD, Seda T, Joester D. Science. 2015; 347(6223):746–750. [PubMed: 25678658]
64. Tamura N, Gilbert PUPA. Methods Enzymol. 2013; 532:501–531. [PubMed: 24188780]
65. Gilow C, Zolotoyabko E, Paris O, Fratzl P, Aichmayer B. Cryst Growth Des. 2011; 11(6):2054–2058.
66. Beniash E, Metzler RA, Lam RSK, Gilbert PUPA. J Struct Biol. 2009; 166(2):133–143. [PubMed: 19217943]
67. Weiner S, Mahamid J, Politi Y, Ma Y, Addadi L. Front Mater Sci China. 2009; 3(2):104–108.
68. Levi-Kalisman Y, Raz S, Weiner S, Addadi L, Sagi I. J Chem Soc Dalt Trans. 2000; No. 21:3977–3982.
69. Weiner S, Addadi L. Annu Rev Mater Res. 2011; 41(1):21–40.
70. Gong YUT, Killian CE, Olson IC, Appathurai NP, Amasino AL, Martin MC, Holt LJ, Wilt FH, Gilbert PUPA. Proc Natl Acad Sci U S A. 2012; 109(16):6088–6093. [PubMed: 22492931]
71. Metzler RA, Tribello GA, Parrinello M, Gilbert PUPA. J Am Chem Soc. 2010; 132(33):11585–11591. [PubMed: 20677733]
72. Metzler RA, Evans JS, Killian CE, Zhou D, Churchill TH, Appathurai NP, Coppersmith SN, Gilbert PUPA. J Am Chem Soc. 2010; 132(18):6329–6334. [PubMed: 20397648]
73. Lam RSK, Metzler Ra, Gilbert PUPa, Beniash E. ACS Chem Biol. 2012; 7:476–480. [PubMed: 22148847]
74. Gamsjaeger S, Mendelsohn R, Boskey AL, Gourion-Arsiquaud S, Klaushofer K, Paschalis EP. Curr Osteoporos Rep. 2014; 12(4):454–464. [PubMed: 25240579]
75. Talari ACS, Movasaghi Z, Rehman S, Rehman I ur. Appl Spectrosc Rev. 2014; 50(1):46–111.
76. Weaver JC, Milliron GW, Miserez A, Evans-Lutterodt K, Herrera S, Gallana I, Mershon WJ, Swanson B, Zavattieri P, DiMasi E, Kisailus D. Science. 2012; 336(6086):1275–1280. [PubMed: 22679090]
77. Amini S, Masic A, Bertinetti L, Teguh JS, Herrin JS, Zhu X, Su H, Miserez A. Nat Commun. 2014 May.5:3187. 2013. [PubMed: 24476684]
78. Lee K, Wagermaier W, Masic A, Kommareddy KP, Bennet M, Manjubala I, Lee SW, Park SB, Cölfen H, Fratzl P. Nat Commun. 2012; 3:725. [PubMed: 22395616]
79. Eder SHK, Gigler AM, Hanzlik M, Winklhofer M. PLoS One. 2014; 9(9):e107356. [PubMed: 25233081]

80. Omelon S, Georgiou J, Variola F, Dean MN. Acta Biomater. 2014; 10(9):3899–3910. [PubMed: 24948547]
81. Lloyd AA, Wang ZX, Donnelly E. J Biomech Eng. 2015; 137(1):010801.
82. Masic A, Bertinetti L, Schuetz R, Galvis L, Timofeeva N, Dunlop JWC, Seto J, Hartmann Ma, Fratzl P. Biomacromolecules. 2011; 12:3989–3996. [PubMed: 21954830]
83. Bennet M, Akiva a, Faivre D, Malkinson G, Yaniv K, Abdelilah-Seyfried S, Fratzl P, Masic a. Biophys J. 2014; 106(4):L17–L19. [PubMed: 24560001]
84. Akiva A, Malkinson G, Masic A, Kerschnitzki M, Bennet M, Fratzl P, Addadi L, Weiner S, Yaniv K. Bone. 2015; 75:192–200. [PubMed: 25725266]
85. Ando T, Kodera N, Naito Y, Kinoshita T, Furuta K, Toyoshima YY. ChemPhysChem. 2003; 4(11): 1196–1202. [PubMed: 14652998]
86. Shibata M, Yamashita H, Uchihashi T, Kandori H, Ando T. Nat Nanotechnol. 2010; 5(3):208–212. [PubMed: 20154686]
87. Kodera N, Yamamoto D, Ishikawa R, Ando T. Nature. 2010; 468(7320):72–76. [PubMed: 20935627]
88. Fukuma T, Jarvis SP. Rev Sci Instrum. 2006; 77(4):043701.
89. Kilpatrick JI, Loh SH, Jarvis SP. J Am Chem Soc. 2013; 135(7):2628–2634. [PubMed: 23398487]
90. Fukuma T, Higgins MJ, Jarvis SP. Biophys J. 2007; 92(10):3603–3609. [PubMed: 17325013]
91. Obst, M.; Schmid, G. Electron Microscopy: Methods and Protocols, Methods in Molecular Biology. Kuo, J., editor. SPRINGER; 233 SPRING ST, NEW YORK, NY 10013 USA: New York: 2014. p. 757-781.
92. Cosmidis J, Benzerara K, Nassif N, Tyliszczak T, Cosmidis J, Benzerara K, Nassif N, Tyliszczak T, Char FB. Acta Biomater. 2015; 12:260–269. [PubMed: 25305511]
93. Li Y, El Gabaly F, Ferguson TR, Smith RB, Bartelt NC, Sugar JD, Fenton KR, Cogswell Da, Kilcoyne aLD, Tyliszczak T, Bazant MZ, Chueh WC. Nat Mater. 2014 Sep 13.:1149–1156. [PubMed: 25218062]
94. Vidavsky N, Addadi S, Mahamid J, Shimoni E, Ben-Ezra D, Shpigel M, Weiner S, Addadi L. Proc Natl Acad Sci U S A. 2014; 111(1):39–44. [PubMed: 24344263]
95. Solomonov I, Talmi-Frank D, Milstein Y, Addadi S, Aloshin A, Sagi I. Sci Rep. 2014; 4:5987. [PubMed: 25100357]
96. Rigort A, Bäuerlein FJB, Villa E, Eibauer M, Laugks T, Baumeister W, Plitzko JM. Proc Natl Acad Sci U S A. 2012; 109(12):4449–4454. [PubMed: 22392984]
97. Rashkovich LN, Yoreo JJ, Orme CA, Chernov AA. Crystallogr Reports. 2006; 51(6):1063–1074.
98. De Yoreo JJ, Zepeda-Ruiz LA, Friddle RW, Qiu SR, Wasylenki LE, Chernov AA, Gilmer GH, Dove PM. Cryst Growth Des. 2009; 9(12):5135–5144.
99. Friddle RW, Weaver ML, Qiu SR, Wierzbicki a, Casey WH, De Yoreo JJ. Proc Natl Acad Sci U S A. 2010; 107(1):11–15. [PubMed: 20018743]
100. Wallace AF, Hedges LO, Fernandez-Martinez A, Raiteri P, Gale JD, Waychunas Ga, Whitelam S, Banfield JF, De Yoreo JJ. Science (80-). 2013; 341(6148):885–889.
101. Sone ED, Weiner S, Addadi L. J Struct Biol. 2007; 158(3):428–444. [PubMed: 17306563]
102. Fang PA, Margolis HC, Conway JF, Simmer JP, Beniash E. J Struct Biol. 2013; 183(2):250–257. [PubMed: 23707542]
103. Fang PA, Conway JF, Margolis HC, Simmer JP, Beniash E. Proc Natl Acad Sci U S A. 2011; 108(34):14097–14102. [PubMed: 21825148]
104. Lucić V, Förster F, Baumeister W. Annu Rev Biochem. 2005; 74:833–865. [PubMed: 15952904]
105. Li D, Nielsen MH, De Yoreo JJ. Methods Enzymol. 2013; 532:147–164. [PubMed: 24188766]
106. Nielsen MH, Li D, Zhang H, Aloni S, Han TYJ, Frandsen C, Seto J, Banfield JF, Cölfen H, De Yoreo JJ. Microsc Microanal. 2014; 20(2):1–12. [PubMed: 24503288]
107. Okuda M, Ogawa N, Takeguchi M, Hashimoto A, Tagaya M, Chen S, Hanagata N, Ikoma T. Microsc Microanal. 2011; 17:788–798. [PubMed: 21899811]
108. Mahamid J, Aichmayer B, Shimoni E, Ziblat R, Li C, Siegel S, Paris O, Fratzl P, Weiner S, Addadi L. Proc Natl Acad Sci U S A. 2010; 107(14):6316–6321. [PubMed: 20308589]

109. Gilbert PUPA. J Electron Spectros Relat Phenomena. 2012; 185(10):395–405.
110. Ma Y, Aichmayer B, Paris O, Fratzl P, Meibom A, Metzler RA, Politi Y, Addadi L, Gilbert PUPA, Weiner S. Proc Natl Acad Sci U S A. 2009; 106(15):6048–6053. [PubMed: 19332795]

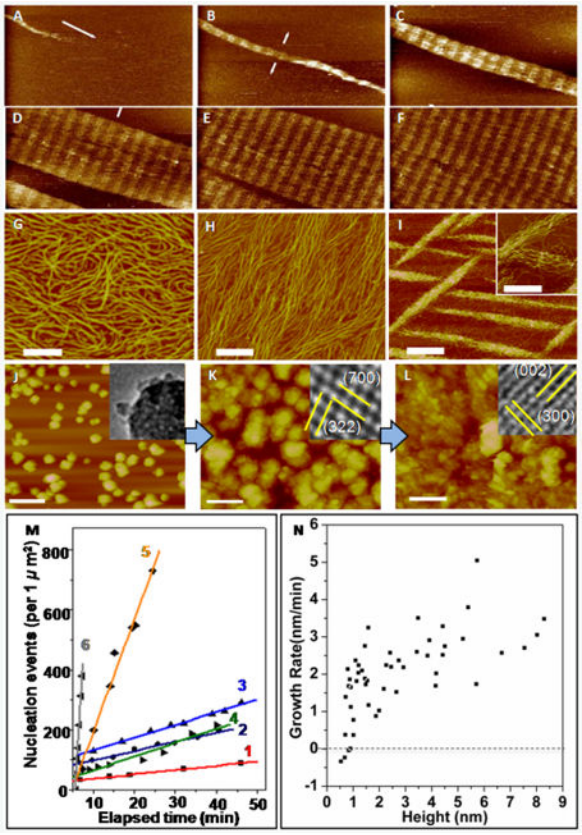

Figure 1.

In situ AFM can be used to investigate matrix self-assembly and mineralization. (A)–(F) Self-assembly of Type I collagen on mica into an ordered array with periodicity of 67 nm found in natural collagen. Times (min) are: (A) 12.9, (B) 25.8, (C) 43.0, (D) 55.9, (E) 60.2, and (F) 77.4. (G)–(I) Architecture of collagen on mica at pH 4.0 for K^+ concentrations (mMol) of (G) 100 (H) 200 (I) 300. (J)–(L) Nucleation of calcium phosphate on collagen at a solute concentration above the ACP solubility limit. (J) ACP at 24 min then transforms to octacalcium phosphate at 64 min (K) and then HA at 98 min (L). Time 0 corresponds to the moment solution was injected into the atomic force microscopy fluid cell. Insets show transmission electron microscopy images collected on samples taken from the three stages of development. (M) Dependence of nucleation rate on time at six different supersaturations σ_i. Details of the supersaturation values can be found in Reference 8. Analysis of the data gives interfacial energies α_i of α_{ACP} = 40 mJ • m^{-2} and α_{HA} = 90 mJ • m^{-2}. (N) Relationship between growth rate and particle height on surface of collagen with σ_{HA} = 3.31, σ_{OCP} = 1.71, σ_{ACP} = –0.02. A critical size of 0.7 nm is determined from the zero crossing of the average growth rate (dashed line) All scale bars are 200 nm except in (I) where it is 500 nm in the main image only. Adapted and reprinted from [8] with permission from Elsevier. Reprinted with permission from Macmillan Publishers Ltd [11]

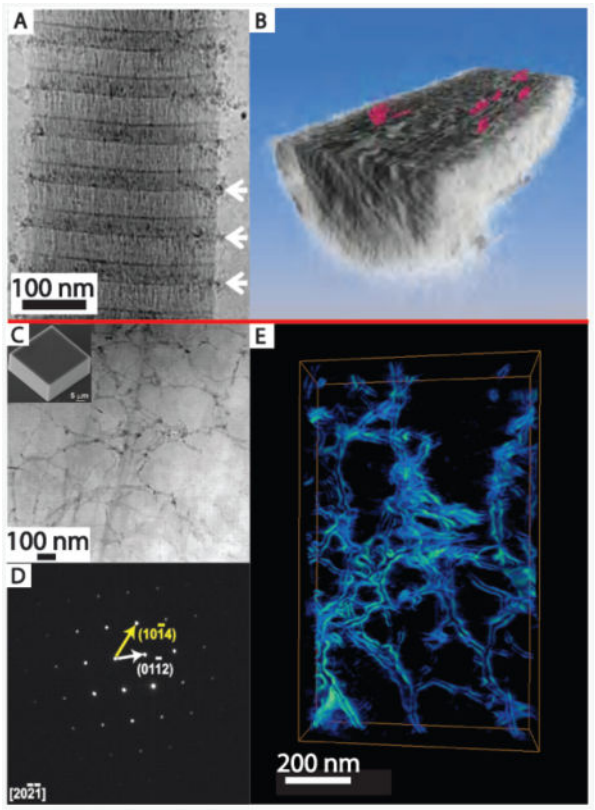

Figure 2.

(A, B) Cryogenic electron microscopy yields insights into the mineralization of hydrated samples. (A) CryoTEM of a collagen fibril (from horse tendon) with amorphous calcium phosphate (ACP) particles collecting near the hole regions of the collagen (white arrows) after mineralization for 24 hrs in buffered $CaCl_2$, KPO_4, and 10 μg/mL of pAsp. (B) Tomographic reconstruction of the fibril after the apatite has been fully crystallized (72 hrs in buffered solution) reveals platelets (colored red) of mineral within the fibril itself. (C)–(E) Electron microscopy and tomography reveal details of incorporated macromolecular additives. (C) ADF-scanning transmission electron microscopy (STEM) of a focused ion beam section of a calcite crystal (scanning electron microscopy, inset) grown in a 1 w/v% agarose gel. Despite well-developed rhombohedral crystal, agarose gel fibers are clearly visible (darker contrast) randomly distributed within the thin section. (D) Selected-area electron diffraction of the area imaged in (C) demonstrating that the gel-grown crystal diffracts electrons as a single crystal. (E) ADF-STEM tomographic reconstruction of an area similar to (C) which emphasizes the network of agarose fibers incorporated within the crystal. Adapted and reprinted by permission from Macmillan Publishers Ltd: [28]. Also from [55] with permission from AAAS

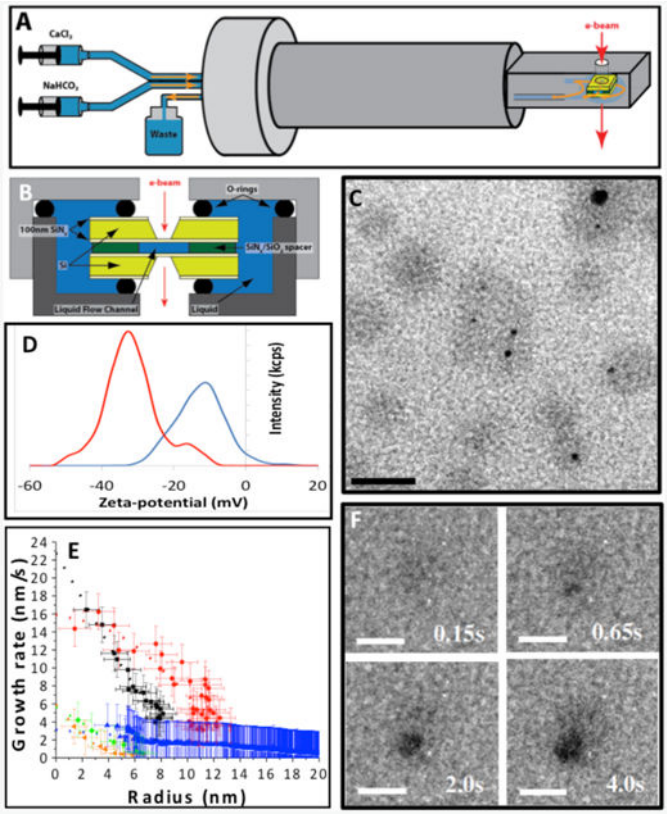

Figure 3.

In situ liquid phase transmission electron microscopy (TEM) enables observation of nucleation and phase evolution for both mineral and organic components. Schematic of (A) TEM liquid cell holder and (B) liquid cell. (C) Globules (gray) formed through Ca^{2+} counter-ion condensation on polystyrene sulfonate (PSS), some containing newly formed amorphous calcium carbonate (ACC) particles (black). (D) Zeta potential showing shift to more positive values due to Ca^{2+} binding to PSS to form globules (red—pure $CaCl_2$ solution, blue— $CaCl_2$ solution containing PSS). (E) Growth rates of vaterite particles (orange, green, blue) formed in the absence of PSS and ACC particles (black and red) within Ca-PSS globules. (F) Time series showing ACC nucleation and growth within a globule. In absence of PSS, vaterite forms randomly (not shown). Scale bars: (C) 50 nm, (F) 20 nm. Adapted and reprinted by permission from Macmillan Publishers Ltd: [35]. Also adapted and reprinted from [34] with permission from AAAS.

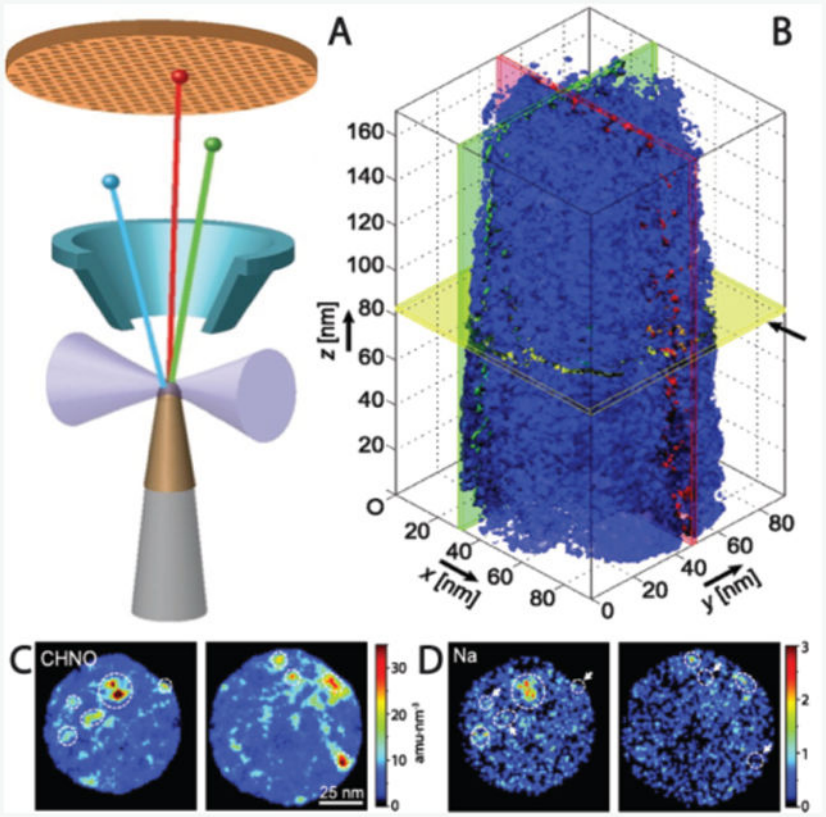

Figure 4.

(A) Schematic of an atom probe tomography experiment in which the sample is ablated by a laser (forming ions) onto a mass spectrometer to determine the type of atoms within the removed section. (B) Tomographic reconstruction of an elephant dentin sample shows the isosurface for the organic fragment number density (blue surface is the threshold for dense organic) revealing fibers aligned along the *z* axis. (C) and (D) Selected sections from the reconstruction in (B) with mass density for organic fragments (C) and Na^+ (D) locations shown. The highest density regions for each are often, but not exclusively, the same, which implies that something in the organic macromolecules may bind the ions. Scale for (C) and (D) are the same as (B) *x*–*y* plane. Adapted and reprinted with permission from [62].

Table I

Summary of the various techniques discussed and brief summary of advantages/disadvantages.

Technique	Benefits	Limitations	References
AFM (ATOMIC FORCE MICROSCOPY)	• Direct visualization of nuclei formation and growth • Direct visualization of incorporation processes • Atomic scale resolution possible	• Specialized set up and difficult Experiments • Limited range of supersaturations • Comparison to bulk studies	3–7, 9, 13, 14, 27, 71–74
CRYOEM	• Maintains hydrated environment • “snap-shots” of dynamic processes	• Specialized sample preparation	19–21, 23, 24, 75–78
LIQUID CELL TEM	• Real-time visualization of nucleation and growth in liquid environment • Possibility to simultaneously image organics	• Emerging technology • Very small reaction volumes • Mixing/trigger of nucleation • Beam artifacts	25–28, 79, 80
(S)TEM AND ELECTRON TOMOGRAPHY	• Direct visualization of organics • Crystallography • 3-D image	• Electron Transparent Sample • Beam Damage • Difficult analysis of 3-D data sets • High vacuum	38, 39, 41, 42, 44–46, 81
IMMUNOGOLD PROTEIN LABELING	• Only technique for direct localization of specific proteins	• Greatly benefited by genomic/ proteomic analysis • Requires antibody for each protein • Limited spatial resolution	34–37
APT (ATOM PROBE TOMOGRAPHY)	• Spatially-resolved chemical information • 3-D image	• Specialized sample preparation and data analysis	47–52
X-RAY SCATTERING BASED MICROSCOPY	• Some chemical mapping ability and correlate small features (e.g., inclusions) to crystallography	• Indirect evidence of organics • Requires synchrotron source • Surface sensitive technique	53–55, 57, 59, 31, 82–84

Technique	Benefits	Limitations	References
	• Bulk samples		
VIBRATIONAL SPECTRO-MICROSCOPY	• Chemically-rich information about organic and inorganic components • Confocal capabilities • Correlation with other techniques • Hydrated samples (only for Raman)	• Auto-fluorescence of some tissues • Resolution limited to 1 μm • For IR, thin, transparent samples	62–66